Wyss, C. R., Rickenmann, D., Fritschi, B., Turowski, J., Weitbrecht, V., Travaglini, E., Bardou, E., Boes, R. M. (2016):Laboratory flume experiments with the Swiss plate geophone bed load monitoring system: 2. Application to field sites with direct bed load samples. - *Water Resources Research*, *52*, pp. 7760—7778.

DOI: http://doi.org/10.1002/2016WR019283

AGU PUBLICATIONS

Water Resources Research

RESEARCH ARTICLE
10.1002/2016WR019283

This article is a companion to *Wyss et al.* [2016], doi:10.1002/2015WR018555.

Key Points:
- Validation of flume-based relations was performed by comparing the predicted number of impulses with those registered in the field
- Using laboratory-based impulse-diameter relations resulted in a calibrated procedure that produces reasonable estimates of the measured bed load masses in the field
- Both stream-specific and stream-independent methods were developed to reproduce the field calibration measurements

Supporting Information:
- Supporting Information S1

Correspondence to:
C. R. Wyss,
carlos.wyss@wsl.ch

Citation:
Wyss, C. R., D. Rickenmann, B. Fritschi, J. M. Turowski, V. Weitbrecht, E. Travaglini, E. Bardou, and R. M. Boes (2016), Laboratory flume experiments with the Swiss plate geophone bed load monitoring system: 2. Application to field sites with direct bed load samples, *Water Resour. Res.*, *52*, 7760–7778, doi:10.1002/2016WR019283.

Received 31 MAY 2016
Accepted 13 SEP 2016
Accepted article online 16 SEP 2016
Published online 9 OCT 2016

Laboratory flume experiments with the Swiss plate geophone bed load monitoring system: 2. Application to field sites with direct bed load samples

Carlos R. Wyss[1,3], Dieter Rickenmann[1], Bruno Fritschi[1], Jens M. Turowski[2], Volker Weitbrecht[3], Eric Travaglini[4], Eric Bardou[4], and Robert M. Boes[3]

[1]Swiss Federal Research Institute WSL, Birmensdorf, Switzerland, [2]Helmholz Centre Potsdam, GFZ German Research Centre for Geosciences, Potsdam, Germany, [3]Laboratory of Hydraulics, Hydrology and Glaciology VAW, ETH Zürich, Zürich, Switzerland, [4]Centre de Recherche sur l'Environnement Alpin CREALP, Sion, Switzerland

Abstract The Swiss plate geophone is a bed load surrogate monitoring system that had been calibrated in several gravel bed streams through field calibration measurements. Field calibration measurements are generally expensive and time consuming, therefore we investigated the possibility to replace it by a flume-based calibration approach. We applied impulse-diameter relations for the Swiss plate geophone obtained from systematic flume experiments to field calibration measurements in four different gravel bed streams. The flume-based relations were successfully validated with direct bed load samples from field measurements, by estimating the number of impulses based on observed bed load masses per grain-size class. We estimated bed load transport mass by developing flume-based and stream-dependent calibration procedures for the Swiss plate geophone system using an additional empirical function. The estimated masses are on average in the range of ±90% of measured bed load masses in the field, but the accuracy is generally improved for larger transported bed load masses. We discuss the limitations of the presented flume-based calibration approach.

1. Introduction

Sediment transport exhibits considerable spatial and temporal fluctuations [*Einstein*, 1937; *Gomez et al.*, 1989], even under hydraulic steady state conditions [*Ancey et al.*, 2015]. These fluctuations are particularly strong in mountain streams where sediment availability plays an important role in relation to bed load transport rates [*Lenzi et al.*, 2004]. For example, when applied to steep gravel bed rivers, empirically based bed load transport formulae tend to overestimate bed load transport rates by one to three orders of magnitude [*Rickenmann*, 2001; *Almedeij and Diplas*, 2003; *Barry et al.*, 2004; *Nitsche et al.*, 2011; *Schneider et al.*, 2015]. This overestimation is also often attributed to the flow resistance produced by the presence of step-pool morphologies and relatively immobile boulders, which can create plunging jets and skimming flows in which energy is dissipated in complex turbulent flow interactions [*Comiti and Mao*, 2012; *Nitsche et al.*, 2012; *Monsalve et al.*, 2016].

Due to the lack of accurate estimations from empirically derived formulae, bed load transport rates in steep gravel bed streams should ideally be measured directly, meaning that bed load is sampled from the natural riverbed. Taking direct bed load samples from a river implies a considerable amount of human effort and time investment, however. Although sophisticated devices able to continuously sample bed load over the whole width of a river like conveyor belts exist [e.g., *Emmett*, 1980; *Hayward*, 1980], they are expensive and their construction is technically challenging. More widely operated direct bed load samplers are mobile and compact, like the Bunte bed load trap [*Bunte et al.*, 2007] or the pressure-difference Helley-Smith sampler [*Helley and Smith*, 1971; *Emmett*, 1980]. They are usually deployed by a person standing on or near the river bed. However, often sampling is difficult or too dangerous during moderate to high flows. In most circumstances, well-designed bed load samplers can provide accurate bed load transport rate measurements, nonetheless, they do not provide continuous measurements and they are generally not operational at high flow discharges, when most of the bed material is mobilized.

To circumvent these limitations, so-called bed load surrogate monitoring techniques have been studied and developed since the 1980s [*Gray et al.*, 2010]. The aim of these newer surrogate monitoring techniques

is not to physically sample transported bed load material, but to measure a byproduct of bed load transport activity with the help of a sensor. Examples include the detection of the acoustic noise created by particle inter-collisions under water [*Thorne*, 1985, 1986; *Belleudy et al*., 2010; *Geay*, 2013] or by measuring microseismic activity along a river reach [*Burtin et al*., 2011].

Field calibration of all bed load surrogate monitoring devices is, until now, necessary to obtain absolute transport rates [*Gray et al*., 2010]. Indeed, particle size and shape as well as hydraulic conditions specific to the field site affect the signal registered by bed load surrogate monitoring technologies [*Thorne*, 1986; *Etter*, 1996; *Bogen and Møen*, 2003; *Esbensen et al*., 2007; *Turowski and Rickenmann*, 2009; *Rickenmann et al*., 2014; *Wyss et al*., 2016a]. The signal registered by the sensor of bed load surrogate monitoring devices is typically complex and contains a broad spectrum of information [*Krein et al*., 2008]. Consequently, to enhance our understanding of the registered signal, characteristic signal values are usually computed. The monitoring device can be calibrated if a significant correlation is found between a computed signal characteristic value, like the number of registered signal peaks or a characteristic signal frequency, and a physical property of the transported bed load like its mass or its particle-size distribution.

Computing characteristic signal values involves signal processing methods that vary in complexity and computational demand. The Japanese pipe hydrophone consists of a hollow steel pipe installed in the riverbed with a microphone monitoring air-pressure differences resulting from colliding bed load impacting on the pipe. *Mizuyama et al*. [2010a] and *Dell 'Agnese et al*. [2014] calibrated the system with the registered pulse rate (computed from the raw signal), which correlates with gravimetric bed load transport rate. However, the relation between the number of registered pulses and transported bed load mass varies for different field sites [*Mizuyama et al*., 2010a]. The difference between field sites can also be observed for other surrogate monitoring systems and is attributed to site-specific hydraulic conditions like mean water flow velocity at the field measuring site [*Rickenmann et al*., 2014], but also to particle size and shape [*Turowski and Rickenmann*, 2009; *Mizuyama et al*., 2010b; *Rickenmann et al*., 2014; *Barrière et al*., 2015], bed load transport rate [*Bogen and Møen*, 2003; *Turowski and Rickenmann*, 2009; *Rickenmann et al*., 2012; *Turowski et al*., 2015], and bed roughness [*Wyss et al*., 2016a].

Other examples of successfully calibrated bed load surrogate monitoring devices are seismometers installed near a river channel. *Burtin et al*. [2008] showed that the seismic signal recorded in the vicinity of a stream is affected both by flowing water (hydrodynamic effects) and by bed load transport activity. They suggested that bed load creep and pebble saltation are responsible for the recorded high frequencies. Their findings agree well with the mechanistic model developed by *Gimbert et al*. [2014], in which seismic noise caused by turbulent flow and seismic noise caused by bed load transport are attributed to lower and higher induced frequencies, respectively. More recently, Roth et al. (D. L. Roth, et al., Sediment transport inferred from seismic signals near a river, submitted to *Journal of Geophysical Research*, 2015) developed a model to estimate bed load transport from a linear inversion of seismic spectra recorded near a steep gravel bed stream with considerable accuracy, i.e., with coefficient of determination R^2 between measured and computed bed load fluxes of about 0.5.

A well-studied bed load surrogate monitoring device is the Swiss plate geophone system which has been used to actively measure bed load transport over decades at the Erlenbach, a steep stream located in the Swiss pre-alps [*Rickenmann and Fritschi*, 2010; *Rickenmann et al*., 2012]. It has also been calibrated in different steep gravel bed rivers to measure bed load transport rates [*Rickenmann et al*., 2012; *Hilldale et al*., 2014; *Rickenmann et al*., 2014]. The applicability spectrum of the Swiss plate geophone spreads from investigating the start and end of bed load transport [*Turowski et al*., 2011], estimating the thickness of the actively transported layer [*Schneider et al*., 2014], demonstrating tools and cover effects related to erosion processes in the field [*Turowski and Rickenmann*, 2009], quantifying the effect of particle size in the energy delivered to the stream bed [*Turowski et al*., 2015] to determining bed load transport by particle-size fractions [*Wyss et al*., 2014, 2016b].

Flume experiments are an ideal tool to quantify the effect of bed load transport determinant parameters on the signal registered by bed load surrogate monitoring devices [*Thorne*, 1985; *Etter*, 1996; *Bogen and Møen*, 2003; *Esbensen et al*., 2007; *Turowski and Rickenmann*, 2009; *Belleudy et al*., 2010; *Mizuyama et al*., 2010b; *Tsakiris et al*., 2014; *Wyss et al*., 2016a]. However, there are only few studies that attempt to compare the signal obtained in the laboratory to that in the field [*Krein et al*., 2008; *Downing*, 2010; *Beylich and Laute*, 2014;

Barrière et al., 2015; *Mao et al*., 2016]. For example, for a system consisting of an impact plate with an accelerometer, *Beylich and Laute* [2014] used their findings from laboratory flume experiments to interpret the signal registered by an uncalibrated device installed in the field. They were able to determine the smallest particle size detectable with their system and to explain some bed load transport dynamics features in two gravel bed rivers. However, lacking field calibration data it is difficult to discuss how well their flume-based calibration can be applied to field conditions.

Using another impact plate system, *Barrière et al*. [2015] performed both flume experiments and field measurements. Based on the flume experiments, they developed a calibration relation to determine the median particle size D_{50} by combining amplitude and frequency information computed from a portion of the signal corresponding to a single particle impact. The range of investigated D_{50} values covered about one and a half order of magnitudes from 2 to 50 mm. When this relation was applied to the field measurements for a flood with bed load transport it predicted a reasonable variation of D_{50} values with changing water discharge.

Recently, data obtained from laboratory flume experiments with the Japanese pipe hydrophone was systematically compared to field calibration measurements [*Mao et al*., 2016]. They were able to establish a reasonable flume calibration of the system, with an R^2 of 0.88 between measured and estimated bed load transport rates. From their flume experiments, they exploited the fact that larger particles trigger larger amplitudes registered by the system [*Mizuyama et al*., 2010b]. Analogous to the packet counts for different amplitude classes with the Swiss plate geophone system used by *Wyss et al*. [2016b], *Mao et al*. [2016] analyzed data from different channels registered by the Japanese pipe hydrophone and developed a calibrated relation to estimate D_{50} of the transported bed load material. When they applied this relation to field measurements, it resulted in a $R^2 = 0.43$ between predicted and measured median particle size D_{50} of the bed load samples.

In this second of two companion papers, we first validate the flume-based relations for the Swiss plate geophone. These relations were obtained in part I of the study [*Wyss et al*., 2016a], in which we determined the number of geophone impulses normalized by bed load mass per grain-size class primarily as a function of particle size and mean water flow velocity. The flume-based relations are validated by comparing the estimated number of impulses with those recorded in the field. This concerns field calibration measurements which were performed earlier in four gravel bed streams: Erlenbach (CH), Navisence (CH), Fischbach (AT), and Ruetz (AT). To do so, the measured bed load masses by grain-size class are combined with the flume-based relations. We then develop two flume-based calibration methods, one site-dependent and one site-independent, that can be used to quantify transported bed load mass in the field for a situation with measured geophone impulses but unknown partitioning of the total bed load into fractions by grain-size class.

2. Methods

2.1. The Swiss Plate Geophone: Signal Characteristics

The Swiss plate geophone is a widely used bed load surrogate monitoring system. It is a robust device that provides accurate bed load transport rate measurements after successful calibration in the field [*Rickenmann et al*., 2012, 2014]. It consists of a steel plate of dimensions 360 mm length, 496 mm width, and 15 mm thickness, horizontally installed over the streambed against which moving bed load particles impact. A geophone sensor (GS-20DX manufactured by Geospace Technologies, Houston, Texas) continuously measures the vibrations of the steel plate at a sampling rate f_s of 10 kHz.

There were digital storage capacity limitations in the field bed load monitoring stations with the Swiss plate geophones when they were installed. Therefore, for regular field measurements, characteristic signal values computed over a given time interval $\Delta_{t,comp}$ (1–15 mi depending on the station) were stored instead of the whole raw signal. For field calibration measurements, $\Delta_{t,comp}$ is typically set to 1 s. So far, only for the Erlenbach stream the raw signal was recorded during the calibration measurements.

The following characteristic signal values are continuously stored at the field stations: The number of impulses *I* recorded over a predefined amplitude-threshold which is related to the number of particle impacts and therefore to the transported bed load mass [*Rickenmann et al*., 2012, 2014]; the maximum positive amplitude during the sampling period *maxA*, which is related to the size of the largest transported particle [*Etter*, 1996;

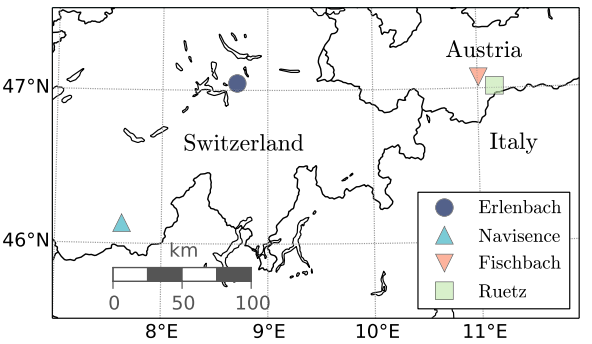

Figure 1. Location of the four streams used in this study for the validation of the flume-based calibration curves for the Swiss plate geophone system.

Rickenmann et al., 2014; *Wyss et al*., 2016b]. Other summary values are also continuously stored [*Rickenmann et al*., 2014], but are not further discussed here because they were not used in this study.

2.2. Field Sites and Field Calibration Measurements

About 20 field sites primarily in Europe, one in Israel, and one in the USA are equipped with Swiss plate geophones. In this study (part II of two companion papers), the flume-based calibration of the Swiss plate geophone obtained in part I [*Wyss et al*., 2016a] are validated with field calibration measurements from the streams given in section 1 (Figure 1). Catchment and channel characteristics of the streams as well as hydraulic and bed load transport properties during the calibration measurements are summarized in Table 1. At the Erlenbach direct bed load samples were taken with automated metal basket samplers with a mesh size of 10 mm and a basket opening of 100 cm by 100 cm, covering the width of two Swiss plate geophones [*Rickenmann et al*., 2012]. At the Navisence, a metal basket with a mesh size of 8 mm and an aperture of the steel frame of the sampler of 50 cm by 50 cm was stabilized directly downstream of one of the 12 geophone plates with the weight of an operator standing on the basket [*Ancey et al*., 2014; *Travaglini et al*., 2014]. At the Fischbach and the Ruetz, bed load samples were taken by deploying a 10 mm mesh-sized basket with an aperture of the steel frame of the sampler of 50 cm by 50 cm stabilized trough a streamlined metal pillar 50 cm downstream of one of the 18 geophone plates [*Rickenmann et al*., 2014]. For comparison purposes, only bed load material from all bed load samples retained by a 10 mm square-spaced sieve is considered in this study.

2.3. Application of Flume-Based Calibration Relations to Field Measurements

A calibration relation is defined here as a function that relates a characteristic signal value δ_v registered by the Swiss plate geophone to bed load particle size D (Figure 2). From our flume experiments performed in near real-scale prototype conditions [*Wyss et al*., 2016a], we obtained different flume-based calibration relations by varying mean flow velocity V_W, bed load material properties (particle shape ζ), and flume-bed sand roughness k_s. Our results show how δ_v varies in relation to these parameters:

$$\delta_v = f(D, V_W, \zeta, k_s)\,. \tag{1}$$

Validation of the flume-based calibration of the Swiss plate geophone is done solely by applying the impulse-diameter relations obtained in the laboratory [*Wyss et al*., 2016a] to the field calibration measurements, without any further calibration step. *Rickenmann et al*. [2014] used the maximum amplitude *maxA* registered over the duration of the calibration measurements $\Delta_{t,sampling}$, to estimate the size of the largest transported bed load particle D_{max}. In general, the recorded *maxA* values depend on the sampling time or recording interval. In contrast, due to its cumulative nature, the information contained in the number of registered impulses I is independent of $\Delta_{t,comp}$, as long as the time interval $\Delta_{t,comp}$ is greater than the duration of an impulse $\Delta_{t,I}$ which in the case of the signal registered by the Swiss plate geophone ranges roughly from 0.3 to 3 ms. This makes I an ideal summary value to measure bed load transport rates and to use it for the comparison of the registered geophone signal from different field sites with different $\Delta_{t,comp}$ and $\Delta_{t,sampling}$ (Table 1).

The laboratory impulse-diameter relation is validated by comparing the impulses registered in the field with the ones computed. To do so, we used field sieved bed load masses per grain-size class from field calibration measurements together with the laboratory impulse-diameter curves (method A).

We additionally developed two purely flume-based approaches that required an additional calibration step and that can be applied in the field for a situation with measured geophone impulses but unknown partitioning of the total bed load into fractions by grain-size class. The first (method B1) requires a stream-specific flume calibration relation, whereas the second (method B2) represents a generalized stream-independent calibration.

Table 1. Catchment and Hydraulic Characteristics at the Field Sites, Partly Summarized From *Rickenmann et al.* [2014]

			Stream			
Parameter		Units	Erlenbach	Navisence	Fischbach	Ruetz
Catchment drainage area		km^2	0.7	82	71	28
Station elevation		m	1 110	1 650	1 540	1 684
Glacier area		%	0	25	17	22
Bed surface D_{50}		mm	70	102	86	98
Bed surface D_{84}		mm	290	228	206	279
Channel width at geophone site		m	1.5[a]	6.0	9.0	9.0
Geology			Flysh	Gneiss	Paragneis[b]	Paragneis[b]
Particle shape ζ[c]			Bladed, angular	Bladed, angular	Bladed, round	Bladed, round
Stream gradient upstream of site		%	16	3	2	5.5
Threshold for impulse count		V	0.1	0.1	0.07[d]	0.07[d]
Field calibration measurements			80	96	28	17
$\Delta_{t,comp}$[e]		s	1	60	1	1
Discharge Q[f]	min.	m^3/s	0.2	2.6	4.8	3.7
	avg.		0.67	6.1	9.5	4.9
	max.		1.53	8.9	17.2	8.7
Unit discharge q[f]	min.	m^2/s	0.13	0.42	0.54	0.41
	avg.		0.45	1.02	1.06	0.54
	max.		1.02	1.48	1.91	0.97
Sampled bed load mass[f]	min.	kg	0.17[g]	0.06[g]	1.50[g]	3.8[g]
	avg.		108[g]	1.76[g]	65.6[g]	23.4[g]
	max.		352[g]	9.4[g]	431.4[g]	128.2[g]
Unit solid transport rate q_b[f]	min.	g/s m	0.27[g]	0.38[g]	4.99[g]	5.94[g]
	avg.		625[g]	16.8[g]	528.5[g]	50[g]
	max.		6 623[g]	100[g]	7 200[g]	213[g]
Mean flow velocity V_W[h]	min.	m/s	4.8	1.8	1.5	1
	avg.		5	2.4	2.2	1.3
	max.		6.5[i]	2.8	2.8	1.9
Water depth h_W	min.	m	0.08[j]	0.24	0.39	0.36
	avg.		0.10[j]	0.41	0.53	0.4
	max.		0.15[j]	0.57	0.72	0.52
Froude number Fr	min.			1.03	0.72	0.61
	avg.		6.1	1.21	0.86	0.66
	max.			1.26	0.99	0.82

[a]An approximated width of 1.5 m was estimated from field observations at the Erlenbach.
[b]The geological overview map also shows a minor presence of orthogneis.
[c]Particle shape ζ was attributed by measuring the three axis of at least 460 bed load particles of each stream [*Wyss et al.*, 2016a] (supporting information). Particle angularity was attributed by comparison with the description from pebbles photographs in *Turowski and Rickenmann* [2009].
[d]Before the impulse count, the raw signal is damped by 30% in these stations.
[e]Interval for computation of signal characteristics.
[f]Values according to those measured during calibration measurements from previously calibrated stage-discharge relationships.
[g]For particle size $D > 10$ mm.
[h]Computed from the continuity equation $V_W = Q/A$, where A is the wetted surface area over the cross section where the geophone plates are installed. At the Erlenbach, A is computed from continuous flow-depth measurements with a 2-D laser sensor TiM551 by SICK AG© installed in spring 2014 [*Wyss et al.*, 2016b]. At the Navisence, Fischbach, and Ruetz, A is computed from the known geometry and the flow-depth measurements provided by the water-stage at the measuring cross section, together with the calibrated discharge data
[i]The maximum mean flow velocity corresponding to the maximum discharge was estimated by a rough interpolation from smaller discharge ranges, i.e., 0.2–1 m^3/s, for which the 2-D laser profile measurements of the water surface provide accurate velocity estimates at the Erlenbach [*Wyss et al.*, 2016b]. Above 1 m^3/s, rainfall starts to have a refracting effect on the laser measurements which makes the determination of A unreliable. Note that the V_W estimated by *Rickenmann et al.* [2014] are inaccurate because 2-D laser profile measurements are available only from May 2014 until September 2015.
[j]Measured with a 2D rotating laser sensor [*Wyss et al.*, 2016b].

2.3.1. Method A: Validation of Flume-Based Calibration Relations With Sieved Field Bed Load Samples

In this approach, validation is done by comparing the number of impulses registered in the field I_{field} with the number of impulses computed with the laboratory impulse-diameter relations I_{flume} based on the measured bed load masses by grain-size class in the field. From our flume experiments [*Wyss et al.*, 2016a], we determined a calibration relation for the parameter k_{bj}, defined as the number of registered impulses divided by the transported mass for particles of a defined grain-size fraction j (Figure 2). These experiments were performed with a wired mesh as bed roughness with an estimated effective sand roughness k_s of 1 mm.

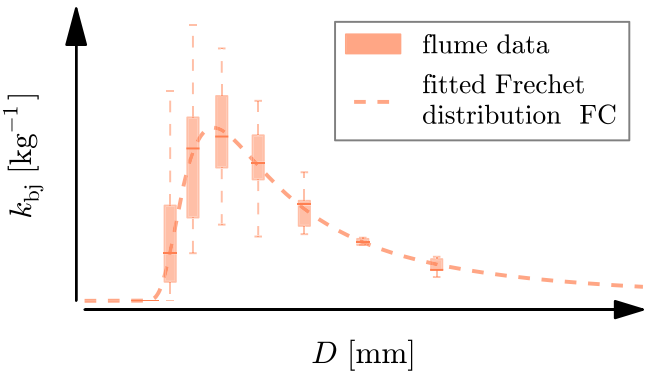

Figure 2. Illustration of an impulse-diameter relation established from laboratory experiments [*Wyss et al.*, 2016a] fitted with a generalized Frechet distribution curve FC.

The values of k_{bj} as a function of D_m for the flume experiments could are well fitted with a generalized Frechet distribution [*Wyss et al.*, 2016a]. The advantage in fitting a curve is that it allows for the computation of impulses I_{flume} independently of the size of the sieved bed load fractions j in the field as:

$$I_{flume} = \sum_{j=1}^{n} k_{bj,flume} \cdot M_{j,field}\,, \qquad (2)$$

where $M_{j,field}$ is the bed load mass of particle size fraction j of a given field sample and $k_{bj,flume}$ is the calibration parameter derived from the flume experiments. There is a strong dependency of $k_{bj,flume}$ on the size of the transported particles D_m (Figure 2), which is computed as the geometric mean of the upper and the lower sieve sizes. Hence, comparing I_{flume} with the number of registered impulses in the field I_{field} for every calibration measurement reveals the accuracy or validity of the established flume-based calibration curve.

2.3.2. Method B1: Development of Purely Flume-Based Calibration Procedure, for Each Stream

This approach consists of the development of a stream-specific procedure, and a final equation, established without any direct knowledge of the transported bed load particle size fraction mass M_j.

The number of impulses registered by the Swiss plate geophone normalized by unit transport mass (k_b values) are mainly affected by two key parameters: the size of the transported particles D and the velocity at which they are transported V_p. Although V_p is difficult to estimate in the field, we assume that it is related to the mean water flow velocity V_W [*Julien and Bounvilay*, 2013]. For our field sites, we determined V_W based on flow depth h_w or discharge Q, the cross section geometry, and available stage-discharge relations (Table 1).

We further use the information about the largest transported particle size D_{max} estimated from the maximum amplitude *maxA* registered during field calibration measurements for each stream [cf. *Rickenmann et al.*, 2014]. The estimated value $D_{max,est}$ is then used as upper integration limit of the fitted Frechet curve FC:

$$I_{field} = k_b \cdot M_{tot} = \frac{\sum_{j=1}^{n} k_{bj,flume} \cdot M_{j,field}}{\sum_{j=1}^{n} M_{j,field}} \cdot M_{tot} = C_{s,i} \cdot M_{tot} \int_{D=0}^{D=D_{max,est}} \mathrm{FC}\, dD\,, \qquad (3)$$

where $C_{s,i}$ is a parameter to be calibrated and i is the number of the field calibration measurement for a given stream s. Given that $\sum_{j=1}^{n} M_{j,field} = M_{tot}$, equation (3) can be rewritten as:

$$C_{s,i} = \frac{\sum_{j=1}^{n} k_{bj,field} \cdot M_{j,field}}{M_{tot} \cdot \int_{D=0}^{D=D_{max,est}} \mathrm{FC}\, dD} = \frac{k_{b,field}}{\int_{D=0}^{D=D_{max,est}} \mathrm{FC}\, dD}\,. \qquad (4)$$

The stream-specific coefficient $k_{b,flume,stream}$ [1/kg] is computed by integrating the particle-size dependent flume-based calibration relation from $D = 0$ to $D = D_{max,est}$:

$$k_{b,flume,stream} = C_s(M_{tot}) \int_{D=0}^{D=D_{max,est}} \mathrm{FC}\, dD\,, \qquad (5)$$

where $\mathrm{FC} = f(D, V_W)$ is the generalized Frechet distribution fitted to the flume-based stream-dependent calibration relation (Figure 2), determined with the closest mean flow velocity V_W to the one estimated in the field (Table 1). The calibration parameter C_s is obtained from an empirical relation fitted to the data of $C_{s,i}$

and M_{tot} for each stream. Total transported bed load mass $M_{tot,est}$ can finally be calculated by an alternative form of equation (3):

$$M_{tot,est} = \frac{I_{field}}{k_{b,flume,stream}} . \quad (6)$$

2.3.3. Method B2: Development of Purely Flume-Based Calibration Procedure, Generalized for All Streams

This approach is analogous to B1, but generalized in the sense that it consists of the development of a stream-independent procedure. The first step is to generalize the Frechet distributions characterizing the calibration curves $\overline{FC} = f(D_j)$, which were obtained for bed material from four streams and for different mean flow velocities V_W. To this end, the parameters defining the fitted Frechet distributions are parametrized as a function of the mean flow velocity V_W. This allows to proceed exactly as in approach B1, but with an impulse calibration coefficient $k_{b,flume,gen}$ generalized for all streams, in which V_W is the single independent variable:

$$k_{b,flume,gen} = C_{gen}(M_{tot}) \int_{D=0}^{D=D_{max,est}} \overline{FC}\, dD , \quad (7)$$

where C_{gen} is, in contrast to method B1, a single empirical relation fitted to the data of $C_{s,i}$ and M_{tot} for all four streams. Total transported bed load mass $M_{tot,est}$ can finally be calculated with:

$$M_{tot,est} = \frac{I_{field}}{k_{b,flume,gen}} . \quad (8)$$

3. Results

3.1. Method A

We compare here the number of impulses registered in the field $I_{field,}$ which is directly related to the transported bed load mass [*Rickenmann et al.*, 2012, 2014], with the number of impulses obtained from the laboratory-based relation for $k_{bj,flume}$ by applying equation (2). For the comparison, we computed the discrepancy ratio r_I for each field calibration measurement as:

$$r_I = \frac{I_{flume}}{I_{field}} . \quad (9)$$

For each of the four streams, I_{flume} was estimated with the flume-based calibration relations for all V_W values for which flume experiments were performed. The results of this comparison are shown in Figure 3 only for the nearest mean flow velocity (between flume and field) and in Table 2 for all mean flow velocities investigated in the laboratory. If we consider the flume conditions closest to the mean flow velocity in the field, the relative standard error of the estimated impulses is in the range of ±55% to 125% for the four streams. On average, the relative standard error is about ±80%. The variability of the discrepancy ratio is further illustrated by box-plots in Figure 3, highlighting a relatively poorer prediction of impulses for the Navisence and Ruetz streams than for the Erlenbach and Fischbach.

3.2. Method B1

Rickenmann et al. [2014] showed that the number of impulses registered by the Swiss plate geophone varies between field sites for the same amount of transported bed load material (Figure 4). From field measurements they determined the calibration coefficient $k_{b,field}$ linking total transported mass M_{tot} to the number of registered impulses:

$$I_{field} = k_{b,field} \cdot M_{tot} , \quad (10)$$

where I_{field} is the number of registered impulses counted above the threshold voltage during the whole sampling time.

Our flume experiments showed that the number of impulses registered by the Swiss plate geophone is highly dependent on the size of the transported particles [*Wyss et al.*, 2016a]. Therefore, to compute a calibration coefficient $k_{b,flume}$ derived from the flume-based calibration curves, some information about the size of the transported particles is necessary. We estimated the size of the largest transported particle $D_{max,est}$ from the maximum registered amplitude *maxA* as in *Rickenmann et al.* [2014]. The relation between the maximum registered amplitude by the Swiss plate geophone over the entire sampling period *maxA* and the

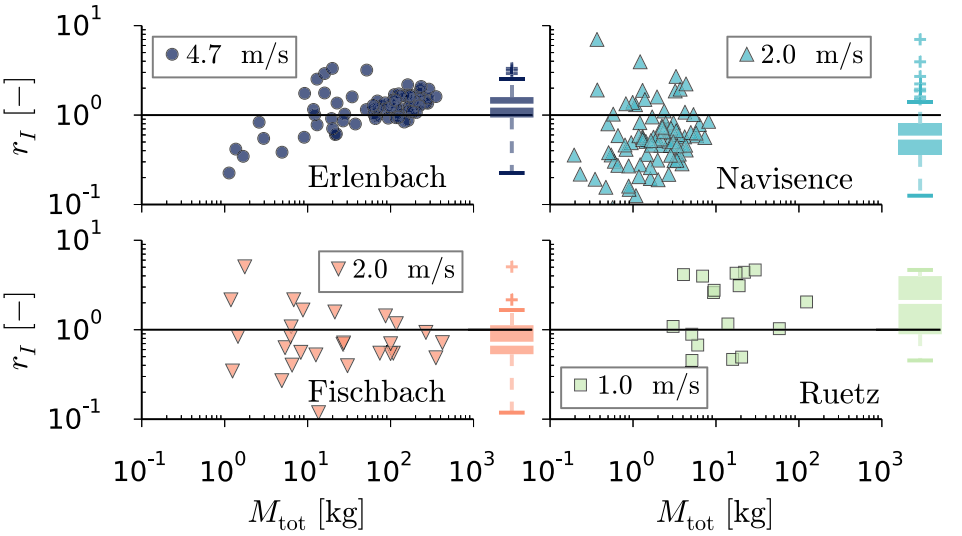

Figure 3. Method A: Ratio of flume-computed to field-measured impulses r_I (equation (9)) for all field calibration measurements, shown as a function of total sampled bed load mass M_{tot}. Here, we show r_I computed with the flume-based calibration relations obtained with the nearest mean flow velocity V_W to that in the field (Table 2). The solid line indicates a perfect agreement. On the right, the boxplots cover the interquartile range IQR and the whiskers the range of ±1.5· IQR from the medians. One data point of the Erlenbach and the Fischbach streams and seven data points of the Navisence have an r_I value smaller than 10^{-1} [–]. These data were left out of this figure to better visualize the considerable scatter around the perfect agreement.

size of the largest measured transported bed load particle D_{max} is reasonably consistent between different field sites [see also *Rickenmann et al.*, 2014] (Figure 5). A power law equation describing the increase in D_{max} as a function of *maxA* for the field calibration measurements at the four sites is used to compute the estimated D_{max} as:

$$D_{max,est} = a_F \cdot \max A^{b_F} . \quad (11)$$

With the coefficient $a_F = 85.5$ [mm/V] and exponent $b_F = 0.41$ [–], equation (11) has a coefficient of determination R^2 of 0.61.

The first step is to calibrate $C_{s,i}$ using equation (4). A further analysis showed that $C_{s,i}$ values decrease with increasing M_{tot} (Figure 6), and an estimated value C_s can be obtained from a power law regression of the data as:

Table 2. Mean Discrepancy Ratio $\bar{r}_I$ (Equation (9)) for all Calibration Measurements Per Stream Obtained for Different Mean Flow Velocities V_W in the Flume [*Wyss et al.*, 2016a] and Its Corresponding Relative Standard Error $\sigma_{e,I}$[a]

Stream	$V_{W,field}$ (m/s)	$V_{W,flume}$ (m/s)	$\bar{r}_I$ (–)	$\sigma_{e,I}$[b] (–)
Erlenbach	5.0	1.5	1.82	1.34
		2.5	0.99	0.40
		3.5	0.75	0.30
		4.7	*1.28*	*0.55*
Navisence	2.4	1.6	0.98	0.78
		2.0	*0.75*	*0.67*
		3.0	0.61	0.66
Fischbach	2.2	1.0	1.78	0.57
		2.0	*0.97*	*0.71*
		3.0	0.85	0.86
Ruetz	1.3	*1.0*	*2.25*	*1.25*
		2.0	1.62	0.88
		3.0	1.09	0.72

[a]The values in italics refer to flume conditions which are closest to the mean flow velocity in the field.

[b]$\sigma_{e,I}$ computed as the standard deviation of the difference between I_{flume} and $I_{field,}$ divided by the average number of impulses registered in the field $\bar{I}_{field}$ for each stream individually.

$$C_s = a_C \cdot M_{tot}^{b_C} . \quad (12)$$

The coefficient a_C [1/kg mm] and exponent b_C [–] in equation (12) vary with bed load material properties and are summarized in Table 3.

Although the correlation between $C_{s,i}$ and M_{tot} is rather weak (Table 3) a power law function seems reasonable to fit each stream independently (Figure 6 and Table 3).

To estimate C_s, equation (12) was applied using as initial value M_{tot} calculated with the number of impulses and an average coefficient $k_{b,field,avg} = 12.6$ 1/kg (Figure 4) for all four streams (Figure 4). The total transported bed load mass $M_{tot,est}$ was then calculated using equations (5) and (6),

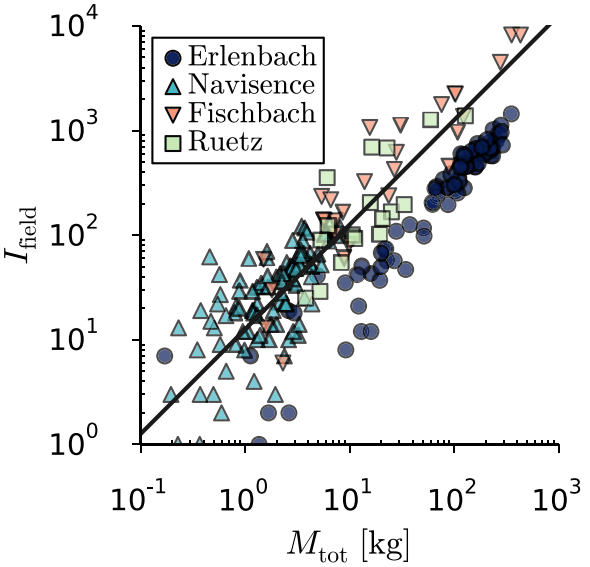

Figure 4. Number of registered impulses in the field I_{field} as a function of total transported bed load mass M_{tot} ($D > 10$ mm). The properties of the calibration measurements are summarized in Table 1. The solid line represents an averaged linear relation between M_{tot} and I_{field} for all four streams, i.e., $k_{\text{b,field,avg}} = 12.6$ 1/kg. Adapted from *Rickenmann et al.* [2014].

together with estimates of the largest transported particles D_{max} from the amplitude of the signal (equation (11)). Using the value $M_{\text{tot,est}}$ the calculation procedure was repeated iteratively, starting with equation (12), and using equations (5) and (6). The calculation procedure was found to converge sufficiently precisely after 10 iteration steps, with an average difference of the $M_{\text{tot,est}}$ values of the last steps of less than 0.1%.

As a measure of prediction accuracy, r_M is defined as the discrepancy ratio of $M_{\text{tot,est}}$, to the measured bed load mass M_{tot}:

$$r_M = \frac{M_{\text{tot,est}}}{M_{\text{tot}}} . \tag{13}$$

Its performance is illustrated in Figure 7 as a function of M_{tot}. The performance of this method is further compared to method B2 through the relative standard error calculated between $M_{\text{tot,est}}$ and M_{tot} for the field calibration measurements (Table 4).

The use of method B1 (Table 4) to estimate total transported bed load mass tends to produce more accurate results for larger transported bed load masses (Figure 7). The discrepancy between estimated measured values appears to be particularly reduced for M_{tot} values larger than about 30 kg. On average, the computed flume-based calibration coefficient $k_{\text{b,flume,stream}}$ is in the range of $\pm 30\%$ of the calibration coefficient measured the field $k_{\text{b,field}}$ (Table 4), but the uncertainty is considerably larger for the data from the Navisence with relatively small M_{tot} values (Figure 7).

3.3. Method B2

The four parameters defining the fitted generalized Frechet distribution describing the impulse-diameter relation of the Swiss plate geophone for bed load material from all four streams were found to vary with the mean flow velocity V_{W} [*Wyss et al.*, 2016a]. As a result, a generalized impulse-diameter relation $\overline{\text{FC}} = f(D_{\text{m}})$ was established using V_{W} as additional variable (Figure 8). The equation and parameters of the generalized Frechet distribution are reported in *Wyss et al.* [2016a].

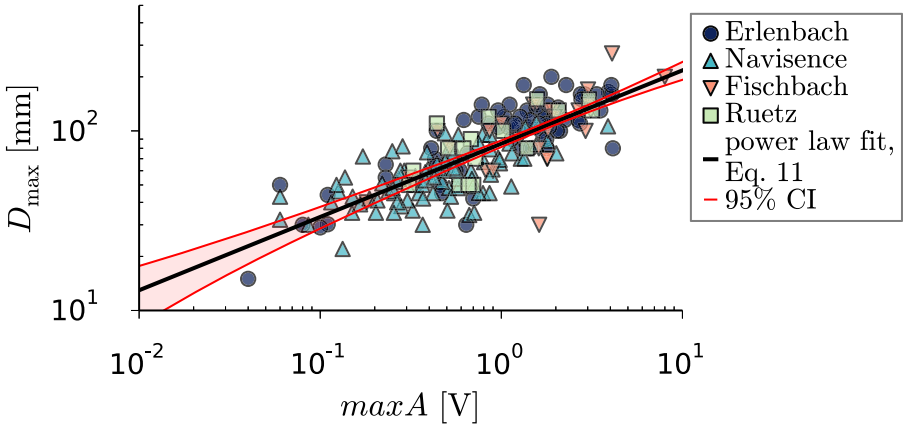

Figure 5. D_{max} as a function of *maxA* for the field calibration measurements. Data from 236 field calibration measurements were used to obtain the power law fit. The red curves indicate the 95% confidence interval CI. To compensate the damping of the geophone signal at the Fischbach and the Ruetz, *maxA* values were multiplied by a factor of 1.3 as in *Rickenmann et al.* [2014].

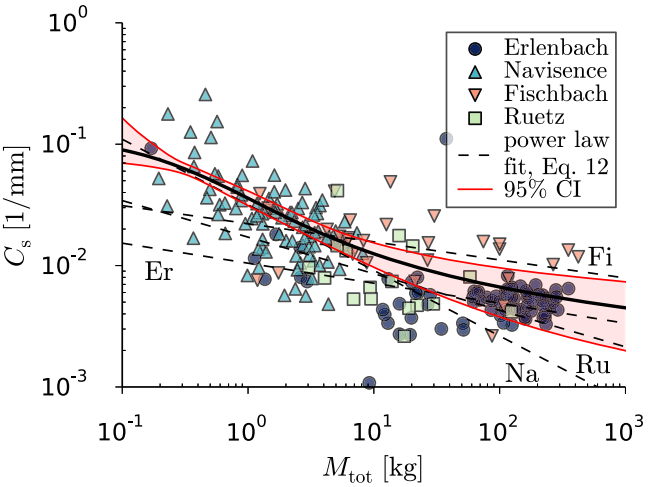

Figure 6. The calibrated parameter C_s (from equation (4)) is shown as a function of M_{tot}. C_s appears to vary also with bed load material properties (Table 3). The solid black line is a general fit obtained with the data from all streams (equation (14)) and the red curves indicate its 95% confidence interval CI.

In this method, a general fit for the data $C_{s,i}=f(M_{tot})$ for the four streams (Figure 6) was obtained applying an equation in the form of:

$$C_{gen}=\frac{a_g}{\left[\log_{10}(M_{tot}+b_g)\right]^{c_g}}. \quad (14)$$

Parameters $a_g=0.013$, $b_g=1.28$, and $c_g=0.98$ with the respective $R^2=0.21$ in equation (14) were determined using a nonlinear least square optimization procedure. The optimization procedure was performed with five equally log-spaced binned data of each stream, such that, even if the streams differ in the number of field measurements (data points) they are equally weighted before fitting equation (14). By doing so, a general calibration coefficient $k_{b,flume,gen}$ can be computed with equation (7). The values of the integral in equation (5) with the stream-dependent parameter FC (B1) and in equation (7) with the stream-independent parameter $\overline{FC}$ (B2) derived from the flume calibration measurements are comparable (Figure 9). Note that for the Navisence and the Fischbach the values of the integral in equation (7) are very similar in method B2 (Figure 9b), because they were computed with the generalized impulse-diameter relation (Figure 8) with a similar V_W value measured in the field (Table 1). The total transported bed load mass was computed using the generalized stream-independent calibration coefficient $k_{b,flume,gen}$ in equation (8) (Figure 10). Results obtained with methods B1 and B2 are summarized quantitatively in Table 4.

The use of approach B2 (Table 4) to estimate total transported bed load mass tends to produce more accurate results for larger bed load masses (Figure 10). The discrepancy between estimated measured values appears to be particularly reduced for M_{tot} values larger than about 30 kg. On average, the relative standard error between the estimated and the measured bed load masses in the field is of order 3 (Table 4). However, this average value of uncertainty is considerably influenced by the relatively poor performance of the method B2 in the case of the Fischbach with a value of 5.54 (Table 4), for which the $C_{s,i}$ values tend to be generally underestimated using equation (14) (Figure 6), resulting in an overestimation of the measured bed load masses in the field (Figure 10).

3.4. The Effect of Bed Roughness

The validation calculations presented in section 3.1 were done with flume-based calibration curves performed over a rough flume bed with a sand roughness $k_s=1$ mm upstream of the geophone. At the Erlenbach and the Navisence streams, the Swiss plate geophones are installed in an artificial concrete bed where the presence of cemented boulder riprap creates some artificial roughness. At the Fischbach and the Ruetz streams, the Swiss plate geophones are mounted in a sill installed across the natural stream bed. Flume experiments with a smooth bed ($k_s=5\times10^{-2}$ mm) were performed additionally with bed material from the Erlenbach. Here we illustrate the effect of bed roughness on the predicted number of impulses by validating the field measurements using impulse-diameter curves obtained with a smooth bed, i.e., a PVC plate upstream of the Swiss plate geophone in the flume [*Wyss et al.*, 2016a]. As in section 3.1, equation (9) was used to compute the number of impulses with the flume-based calibration relations, obtained both with a rough and a smooth flume bed (Figure 11).

Table 3. Coefficient a_C and Exponent b_C in Equation (12) With Respective Coefficient of Determination R^2 for the Different Streams

Stream	a_C (1/mm)	b_C (–)	R^2 (–)
Erlenbach	0.010	−0.165	0.25
Navisence	0.032	−0.558	0.43
Fischbach	0.022	−0.149	0.16
Ruetz	0.017	−0.301	0.19

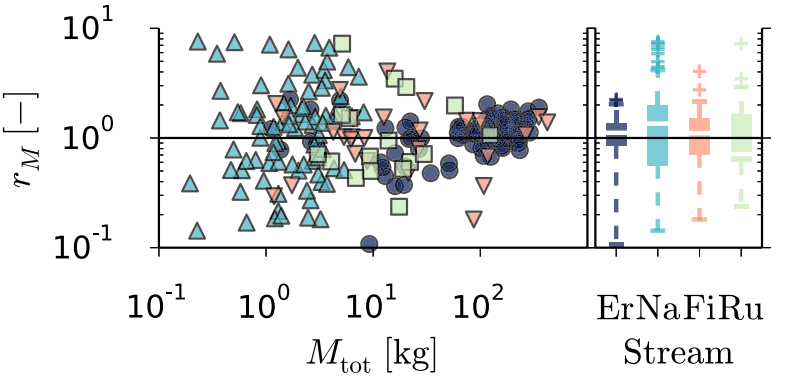

Figure 7. Method B1: Ratio r_M of estimated to measured bed load mass as a function of measured bed load mass M_{tot}. $M_{tot,est}$ was estimated with equations (5) and (6) and the stream-specific relations $C_s = f(M_{tot})$. On the right, the boxplots cover the interquartile range IQR and the whiskers the range of $\pm 1.5 \cdot$ IQR from the median. Three data points of the Erlenbach and seven data points of the Navisence have an r_I value either larger than 10^1 [–] or smaller than 10^{-1} [–]. These data were left out of this figure to better visualize the considerable scatter around the perfect agreement.

The level of accuracy is illustrated by the discrepancy ratio between computed and measured number of impulses r_I (equation (9)) and the relative standard error $\sigma_{e,I}$ (Table 5). This comparison mainly indicates that with a smooth bed the flume-based calibration results in a considerable underestimation of the number of impulses measured in the field.

4. Discussion

4.1. Comparability of Signal Response Between Field and Laboratory Systems

To enable a direct comparison between the signal response in the laboratory and in the field, a projectile ball was dropped from different heights over the center of the Swiss plate geophone installed in the laboratory flume and at the Erlenbach stream. The ball has a mass of 144 g and is made of a hard rubber with a steel center and has previously been used to determine the energy transfer to the geophone plate [*Turowski and Rickenmann*, 2009; *Turowski et al*., 2013]. The ball was dropped 5 times from 10, 30, 50, 100, 250, 500, and 1000 mm height above the plate's center and recovered after the first bounce. The complete signal response of Swiss plate geophone following a single impact is assumed to be contained within a packet [*Wyss et al*., 2016a]. The maximum positive amplitude within a packet $A_{max,P}$ registered at the different drop heights is a metric that can be compared for the Swiss plate geophones installed in the laboratory flume and in the field at the Erlenbach. It was not possible to perform drop tests over the Swiss plate geophones at the other sites, because in contrast to the Erlenbach there is a minimum water discharge during the entire year that continuously covers the plates. The comparison of the signal response reveals that there is some systematic deviation between the maximum amplitude recorded in the field $A_{max,P,field}$ and in the laboratory flume $A_{max,P,flume}$, as determined from the drop tests (Figure 12):

Table 4. Field-Measured and Flume-Based Mean Calibration Coefficients $k_{b,field}$, $k_{b,flume,stream}$, and $k_{b,flume,gen}$ [a]

Stream	$k_{b,field}$ (1/kg)	$\sigma_{e,M_{tot},k_{b,field}}$ (–)	$k_{b,flume,stream}$ [b] (1/kg)	$\sigma_{e,M_{tot},k_{b,flume,stream}}$ [b] (–)	$k_{b,flume,gen}$ [c] (1/kg)	$\sigma_{e,M_{tot},k_{b,flume,gen}}$ [c] (–)
Erlenbach	3.41	0.24	2.99	0.53	5.68	0.91
Navisence	15.28	0.96	20.15	2.39	22.79	1.01
Fischbach	19.13	0.41	19.45	0.82	10.42	5.54
Ruetz	12.67	0.80	13.71	0.93	23.15	0.69
Together		0.39		0.83		3.01

[a]The relative standard error $\sigma_{e,M_{tot}}$ was computed as the standard deviation of the difference between $M_{tot,est}$ and M_{tot}, divided by the average bed load mass M_{tot} for each stream individually. The relative standard error computed with field measurements $\sigma_{e,M_{tot},k_{b,field}}$ and method B1 $\sigma_{e,M_{tot},k_{b,flume,stream}}$ and B2 $\sigma_{e,M_{tot},k_{b,flume,gen}}$ are an indicator of the method's accuracy. Data points exceeding 10 times the standard deviation of the ratio between estimated and measured bed load masses r_M were considered as outliers (Figures 7 and 10) and were discarded for the computation of the mean calibration coefficients.
[b]Computed with method B1.
[c]Computed with method B2.

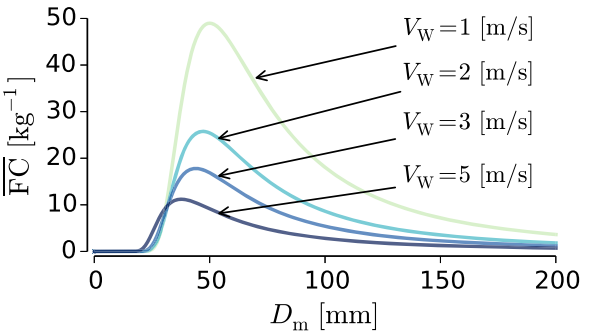

Figure 8. Generalized impulse-diameter calibration $\overline{\mathrm{FC}}=f(D_\mathrm{m})$ plotted for different mean flow velocities V_W.

$$\mathrm{median}(A_{\mathrm{max,P,field}})=a_A \cdot \mathrm{median}(A_{\mathrm{max,P,lab}})^{b_A}. \quad (15)$$

With $a_A=1.06$ and $b_A=0.79$, equation (15) has a coefficient of determination $R^2=0.996$.

Up to about 1 V, the Swiss plate geophone system in the field (Erlenbach) registers higher amplitudes than in the laboratory flume. The reasons for this discrepancy in signal response are not known. In principle, a standard design of the Swiss plate geophone system is used at all sites: the same or very similar dimensions of the stainless steel plates, the same rubber elements for the acoustic isolation, and very similar systems to screw the plates onto a metal framework. This latter part, the metal framework, is not exactly the same at each field site: It is identical in the Fischbach and Ruetz streams, but slightly different in the Erlenbach and the Navisence stream. The system used in the flume is more comparable to those in the Erlenbach and Navisence than to those in the Fischbach and Ruetz. In addition, the number of plates screwed to the same metal framework differs somewhat from stream to stream, and in the flume the metal framework holds only one single plate. Finally, the strength of the screw fixing is unknown at most sites. At the moment we can only speculate that some of these latter factors may be responsible for the different signal response as documented between the Erlenbach and the flume system used in this study.

A power law function describes the increase of the largest transported bed load particle D_max as a function of the maximum registered amplitude *maxA* in the field (Figure 5). The exponent of this function (equation (11)) is in agreement with the one obtained from flume experiments performed with bed load material from the same four streams [*Wyss et al.*, 2016a] (0.41 and 0.40, respectively). The coefficient in equation (11) for field data is in average, however, about 25% larger than the one obtained from flume experiments (85.5 and 67.5, respectively). This is possibly due to the systematic deviation in signal response between laboratory and field systems, for which we showed above that at least at the Erlenbach, the registered amplitudes below 1 V are higher in the field that in the laboratory flume for the same triggering mass (Figure 12).

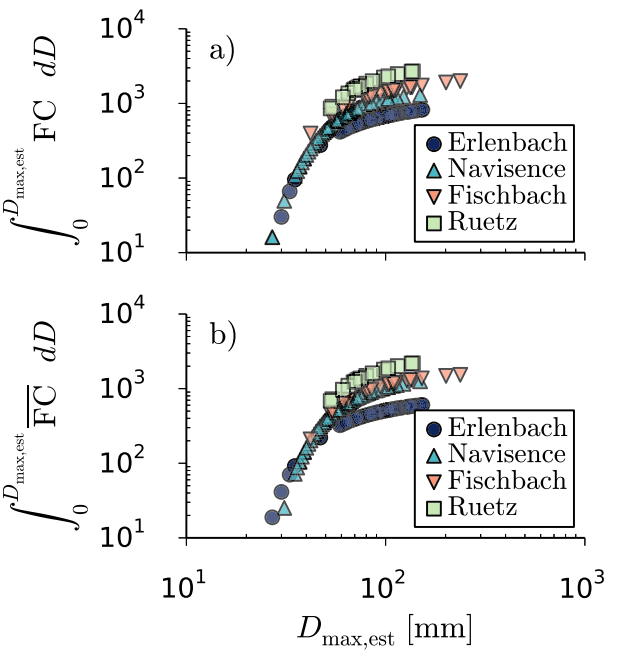

Figure 9. Value of the (a) integral in equation (5) computed with the laboratory impulse-diameter relation for every stream independently (method B1) and (b) the integral in equation (7) computed with the generalized stream-independent laboratory impulse-diameter relation (method B2).

4.2. More Detailed Analysis Considering Grain-Size Classes

Wyss et al. [2016b] defined a parameter α_p as the number of registered packets within a given amplitude range divided by the number of transported particles in the corresponding particle size class, which was included in a procedure to determine bed load transport by grain-size fraction at the Erlenbach stream. The α_p parameter for the field data can only be computed for the Erlenbach because at the other field sites used in this study, the raw signal was not registered during field calibration measurements.

Using the procedure described in *Wyss et al.* [2016a], it is possible to compute equivalent α_p from the flume experiments,

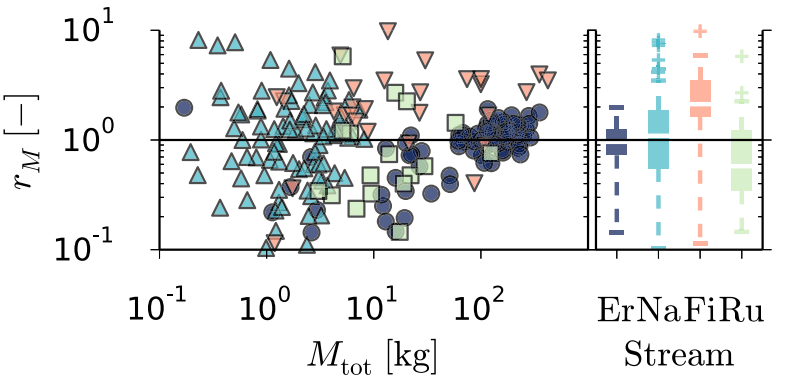

Figure 10. Method B2: Ratio r_M of estimated to measured bed load mass as a function of measured bed load mass M_{tot}. $M_{tot,est}$ was estimated with equations (5) and (6) and the stream-independent relation $C_{gen}=f(M_{tot})$. On the right, the boxplots cover the interquartile range IQR and the whiskers the range of ±1.5· IQR from the median. Five data points of the Erlenbach and seven data points of the Navisence have an r_I value either larger than 10^1 [–] or smaller than 10^{-1} [–]. These data were left out of this figure to better visualize the considerable scatter around the perfect agreement.

by connecting the signals obtained for different particle sizes, so that the final concatenated signal corresponds to that of an averaged bed load sample at the Erlenbach stream. As expected, the relative number of registered packets decreases with increasing flow velocity, up to a mean particle size of about 80 mm. Similarly to the results from the field calibration measurements at the Erlenbach [*Wyss et al.*, 2016b], the α_p values increase with increasing particle size D_m for the flume experiments. However, α_p computed from the flume experiments is clearly larger than the values computed from field calibration measurements (Figure 13). This result cannot be explained with help of the performed drop tests (Figure 12) since one would expect that a smaller number of packets per transported particles α_p should be detected in the lab, especially for particles smaller than about 80 mm which roughly correspond to an amplitude of 1 V (Figure 5) in the field. This might indicate that the wired mesh used as bed roughness for the flume experiments in the lab by *Wyss et al.* [2016a] is not sufficiently adequate to simulate field bed roughness. A smaller α_P value in the field (Figure 13) than in the laboratory, together with the fact that the amplitude of the signal in the field is generally higher than in the laboratory (Figure 12), can be interpreted such that on average, less particles collide against the Swiss plate geophone in the field than in the laboratory. The high mean flow velocities V_W measured at the Erlenbach might generate high turbulent intensities and flow structures different from those that were present in the laboratory, which might be responsible for this effect.

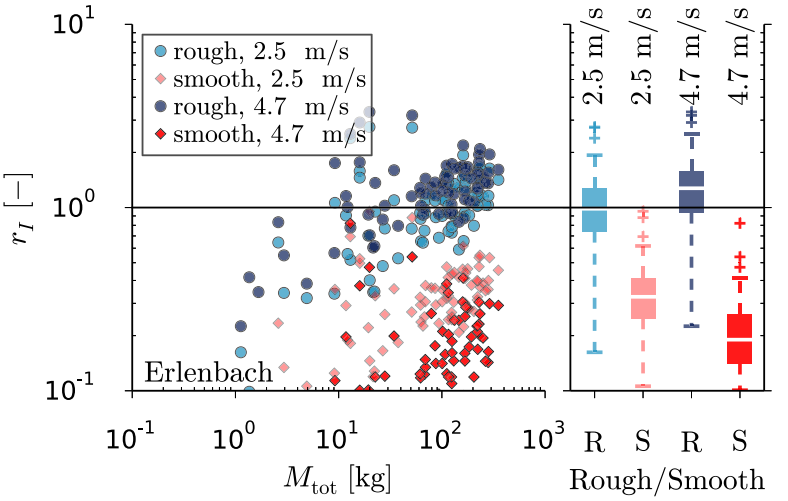

Figure 11. Ratio of computed impulses flume to field-measured impulses r_I (equation (9)) for all field calibration measurements at the Erlenbach, as a function of total sampled bed load mass M_{tot}. Computed impulses are based on flume experiments with both a smooth and a rough bed, and two different mean flow velocities. On the right, the boxplots cover the interquartile range IQR and the whiskers the range of ±1.5· IQR from the median. One data point of rough 2.5 m/s, 3 of rough 4.7 m/s, 4 of smooth 2.5 m/s, and 21 of smooth 4.7 m/s have an r_I value smaller than 10^{-1} [–]. These data were left out of this figure to better visualize the considerable scatter around the perfect agreement.

Table 5. Mean Discrepancy Ration $\bar{r}_I$ (Equation (9)) Obtained With a Rough and a Smooth Flume Bed

Stream	$V_{W,field}$ (m/s)	$V_{W,flume}$ (m/s)	Flume Bed Roughness	$\bar{r}_I$ (–)	$\sigma_{e,I}$[a] (–)
Erlenbach	5.0	2.5	Rough	1.13	0.88
		4.7		1.40	0.90
		2.5	Smooth	0.37	0.89
		4.7		0.20	0.78

[a] $\sigma_{e,I}$ computed as the standard deviation of the difference between I_{flume} and $I_{field,}$ divided by the average number of impulses registered in the field $\bar{I}_{field}$.

It is evident from Figure 13 that there is a systematic overestimation of the number of packets as determined from the flume experiments when compared to the field calibration measurements. This is in quantitative agreement with the result from the validation of the flume experiments for the Erlenbach bed load material (for a mean flow velocity of 4.7 m/s), in which case the number of impulses are overestimated on average by a factor of 1.28 when compared to the number of impulses recorded during the field calibration measurements in the Erlenbach (Table 2).

4.3. Fluid and Particle Velocity Effects

Particle size D, shape ζ, and mean flow velocity V_W have an effect on the signal registered by the Swiss plate geophone system [*Turowski and Rickenmann*, 2009; *Rickenmann et al*., 2014; *Wyss et al*., 2014, 2016b; *Rickenmann et al*., 2014]. In this study, flume experiments were performed:with natural bed load particles from each stream (D and ζ) and by replicating prototype values of the mean flow velocity V_W in the laboratory flume.

By doing so, we established flume-based relations of the system, in terms of $I=f(D,V_w)$. Our validation results (section 3.1) show that the flume-based estimations of impulses are on average within a factor of about two of the field measurements, with a standard error of 55–125% (Table 2). Some systematic divergence in the registered amplitude between field and laboratory systems discussed above can partly explain this discrepancy. However, our flume experiments [*Wyss et al*., 2016a] show that bed roughness k_s affects the geophone signal and has an important effect on the number of registered impulses I per transported unit bed load mass (Figure 11). This suggests that in future, a more precise replication of the field site dependent k_s value and of the hydraulic conditions in the flume could increase the validity of laboratory flume-based calibration approaches when applied to field sites.

For example, bed load particle velocity V_p, and not V_W, is expected to be the governing parameter affecting the number of registered impulses by the Swiss plate geophone system, as it determines particle motion, together with near-bed turbulence conditions. Bed load particles traveling in a fluid are always slower than the surrounding fluid's velocity termed as slip. The slip on planar beds is thus much smaller compared to alluvial bed data where both particle deposition and entrainment phases may intermittently occur [e.g., *Ancey et al*., 2003; *Lajeunesse et al*., 2010]. Indeed, *Chatanantavet et al*. [2013] found that V_p of saltating bed load particles are 20–40% lower than V_W on planar and alluvial beds.

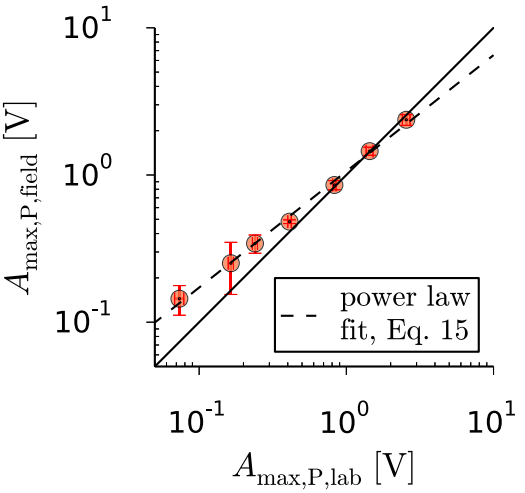

Figure 12. The maximum amplitude of the signal registered at the Erlenbach $A_{max,P,field}$ versus the maximum amplitude of the signal registered in the Laboratory flume $A_{max,P,flume}$ from drop tests performed over 10, 30, 50, 100, 250, 500, and 1000 mm height. Increasing amplitude values correspond to increasing drop heights. The error bars indicate the standard deviation. The solid line indicates a perfect agreement.

For this study, we used V_W as a proxy of V_p. The flume experiments indicated a general decrease in registered impulses with increasing V_W values. This is (at least) in qualitative agreement with an earlier analysis of the field calibration measurements with the geophone system [*Rickenmann et al*., 2014]. This is convenient, because V_W can easily be estimated both in the laboratory and in the field. Due to technical limitations, the flow depths h_W used in the flume experiments were about 10 cm [*Wyss et al*., 2016a]. In contrast, with the exception of the Erlenbach, h_W was considerably larger in the field

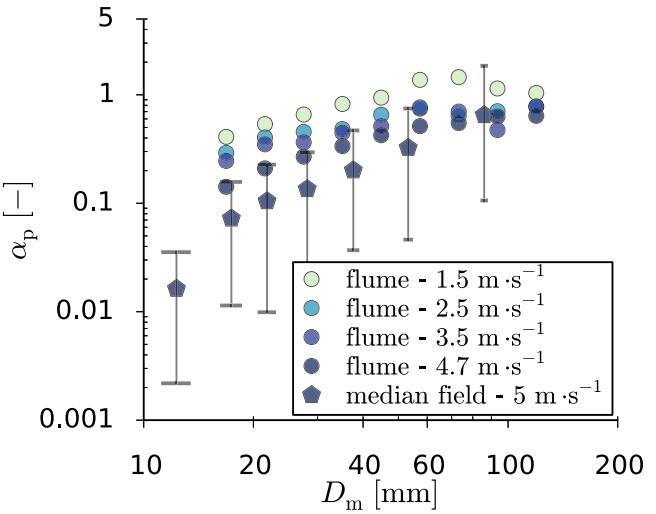

Figure 13. Number of registered packets α_p within a defined particle size class (corresponding to an amplitude range for the field data) divided by the number of particles in the corresponding particle size class computed for field calibration measurements at the Erlenbach and for the flume experiments of *Wyss et al.* [2016a]. The error bars indicate the interquartile range computed from 46 field calibration measurements [*Wyss et al.*, 2016b]. Flume data lacks of error bars because α_p was computed from an artificial signal obtained by concatenating individual particle-size specific signals [*Wyss et al.*, 2016a] to simulate one averaged bed load sample at the Erlenbach.

during the calibration measurements, ranging from 40 to 50 cm at the three other considered field sites (Table 1). For non highly turbulent flow conditions in which a smooth vertical logarithmic velocity profile is expected to develop, differences in particle relative submergence between the flume and the field are translated into different resulting V_p. Vertical velocity profiles are unknown both in the laboratory and field, making it difficult to quantify the potential effect of relative submergence on V_p.

4.4. Impact Location and Particle Size Effects

Figure 6 shows considerable scatter between C_s and M_{tot} for all streams. This is also reflected by the variance in the impulse-based field calibration for total transported bed load mass M_{tot} (Figure 4), and the variance in the estimation of the largest transported particle $D_{max,est}$ from *maxA* (Figure 5), which are both used to compute C_s (equation (4)). We suggest that this variance is due to particle impact location on the geophone plate [*Turowski et al.*, 2013] as well as particle size and shape [*Turowski and Rickenmann*, 2009; *Wyss et al.*, 2016a] and particle transport mode [*Wyss et al.*, 2016a], all having an effect on the number of impulses and the maximum amplitude registered by the Swiss plate geophone system. Variance due to the size of the intake's opening of the samplers (section 2.2) is uncertain. An estimated size of the largest transported particle $D_{max,est}$ within each calibration sample is used as a calibration parameter in methods B1 and B2 (equations (5) and (7), respectively). We presume that the effect of the sampler's intake size is limited due to: (i) only for 4 of the 231 considered samples, the measured D_{max} was larger than one third of the intake's opening; (ii) the trend between sampled D_{max} and *maxA* is consistent between flume experiments and field data (see also section 4.1).

According to equations (12) and (14), the estimated $k_{b,flume}$ values tend to decrease for larger bed load masses. The reason for this is probably that the right-hand part of the Frechet-curve function in Figure 2 becomes more important for larger proportions of coarser transported particles. This tendency is also in agreement with the empirical evidence from the Erlenbach, where somewhat smaller $k_{b,field}$ values were found from the analysis based on the sediment retention basin surveys, as compared to the analysis based on the moving basket samples [*Rickenmann et al.*, 2012]. Our flume-based method B1 appears to partly explain the difference between the moving basket calibration and the retention basin calibration at the Erlenbach (Figure 14), supporting the validity of our flume-based analysis.

4.5. Potential Improvements of Study Setup

Based on the findings of our study, we propose to consider the following elements to further improve a transfer of a flume-based calibration procedure of the Swiss plate geophone system to field conditions: first, future flume experiments should be performed under (real) prototype conditions, i.e., using the same bed material or bed roughness and the same (range of) flow depths and (similar) vertical velocity profiles as at the field sites (apart from using the same particles as in the field). Second, for future field calibration measurements the raw signal should be recorded, to allow for a more sophisticated data analysis and comparison with the flume measurements [cf., *Wyss et al.*, 2016b] (section 4.2). Third, systematic tests should be designed and performed to compare the signal response at the different sites and to systematically quantify

differences from plate to plate (sensor to sensor), not only between field and flume sites, but also for multiple plates at a given field site.

There is one study that successfully compared independent calibration relations for an acoustic bed load measuring technique based on both flume and field measurements. For the Japanese pipe hydrophone system, *Mao et al.* [2016] found that using pulses recorded by the channel with the lowest sensitivity, similar calibration relations resulted between pulses and bed load transport rates from both the flume and field data. However, when applying a calibrated procedure to estimate D_{50} of the transported bed load material derived from the flume measurements to the field, this resulted in relatively poor estimates of the D_{50} observed in the field.

5. Conclusions and Outlook

In this second of two companion papers, we compared and validated flume-based calibration relations between impulse and grain diameter for the Swiss plate geophone system with field calibration measurements. The flume-based relations were obtained in part I of this study [*Wyss et al.*, 2016a].

Our results indicate that a flume-based calibration procedure for the Swiss plate geophone is possible. We applied the flume-based calibration procedures to four field sites with geophone measurements in gravel bed streams. The presented stream-specific predictions of bed load masses are associated with an accuracy in the range of a factor of two of the measured bed load masses (method B1). Given that bed load transport formula can overestimate bed load transport rates by one to three orders of magnitude in (steep) gravel bed streams [*Rickenmann*, 2001; *Almedeij and Diplas*, 2003; *Barry et al.*, 2004; *Nitsche et al.*, 2011; *Schneider et al.*, 2015], this is considered to be a useful step forward. Our flume-based and generalized stream-

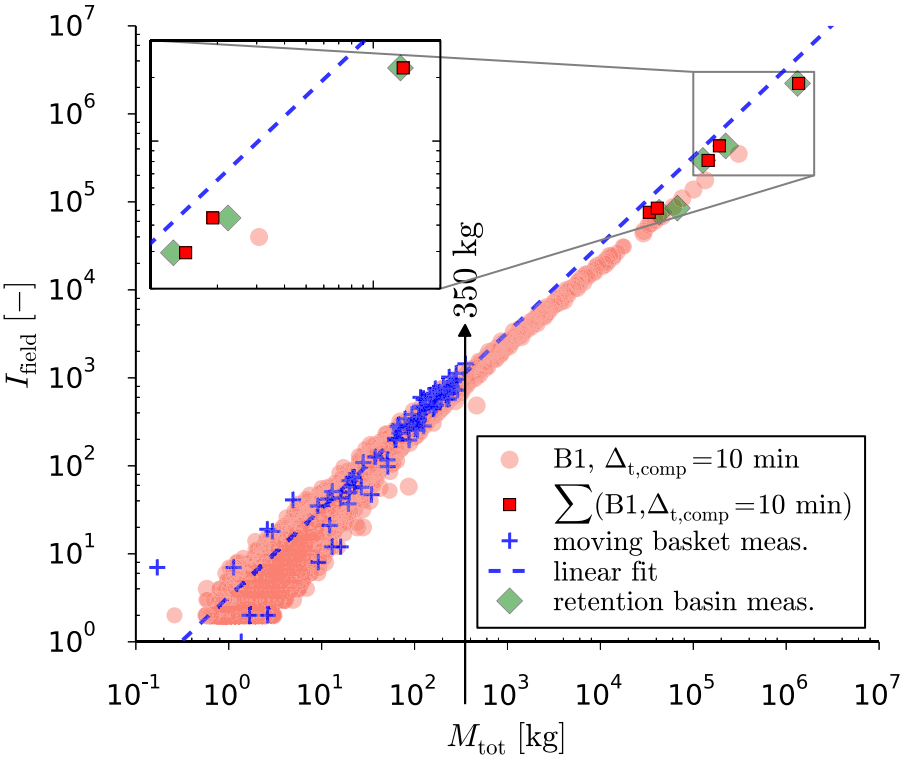

Figure 14. Number of registered impulses as a function of total transported bed load mass ($D > 10$ mm) at the Erlenbach. The dashed blue line indicates a linear fit ($I_{\mathrm{field}} = 3.27 \cdot M_{\mathrm{tot}}$) for the field calibration measurements performed with automated basket samplers [*Rickenmann et al.*, 2012]. The red circles represent back-calculated bed load masses with method B1, using 10 min interval geophone data (impulses and maxima). The green diamonds are observed bed load masses of particles larger than 10 mm determined from the sediment deposit surveys in the retention basin and measured geophone impulses during the same period. The red squares represent estimated bed load masses for the same survey periods, calculated with method B1 using the geophone data. For large values of M_{tot}, an extrapolation of the linear fit obtained from the basket samples (dashed blue line) result in a considerable underestimation of the transported mass. The calculated masses with method B1, however, are in better agreement with the observed sediment deposits.

independent calibration (method B2) can also be applied to uncalibrated field sites, where only impulses and maximum amplitude are recorded, but with a reduced accuracy of about a factor of three relative to the measured bed load masses.

The true potential of a flume-based calibration procedure is to completely replace expensive and exhaustive field calibration measurements. This would make the installation of the Swiss plate geophone system more attractive for scientists and for stakeholders having to deal with strategies concerning sediment management, like hydropower companies and governmental authorities responsible for flood protection. Our study revealed some limitations regarding the transfer of findings from the flume to field conditions. To improve the accuracy of a flume-based calibration procedure for the Swiss plate geophone system, we propose to perform further experiments using real prototype flow conditions including bed roughness, record the raw signal for future field calibration measurements, and test systematically the signal response for plates installed at different sites.

Notation

$A_{max,P,field}$	maximum packet amplitude registered in the field (Erlenbach).
$A_{max,P,flume}$	maximum packet amplitude registered in the flume.
α_p	number of registered packets per transported number particles.
D	particle size.
D_{max}	largest measured particle size.
$D_{max,est}$	largest estimated particle size.
$\Delta_{t,comp}$	time interval for computation of signal characteristics.
$\Delta_{t,I}$	duration of an impulse.
δ_v	characteristic signal value.
Fr	Froude number.
h_w	water depth.
I_{field}	impulses registered in the field.
I_{flume}	impulses registered in the flume.
$k_{b,field}$	field impulse-based calibration coefficient.
$k_{b,flume,gen}$	flume impulse-based and site-independent calibration coefficient.
$k_{b,flume,stream}$	flume impulse-based and site-dependent calibration coefficient.
k_s	bed roughness.
$maxA$	maximum recorded amplitude within a field calibration measurement.
M_{tot}	total transported bed load mass.
Q	discharge.
Q_s	bed load transport rate.
q	unit discharge.
q_b	unit bed load transport rate. r_M: discrepancy ratio between estimated and measured bed load masses.
V_W	mean flow velocity. ζ: particle shape.

Acknowledgments
The authors thank numerous colleagues of the Mountain Hydrology research unit at WSL for their help in the field. The authors are grateful to the Tyrolean Hydro-Power Company (TIWAG) for performing field calibration measurements in the Fischbach and Ruetz streams. Data from the Navisence stream comes from a joint research program conducted at the Centre de Recherche sur l'Environnement Alpin (CREALP) and the Environmental Hydraulics Laboratory (LHE) at the Swiss Federal Institute of Technology in Lausanne (EPFL), with the financial support from the commune d'Anniviers, in the canton of Valais, Switzerland. This study was supported by the Swiss National Science Foundation SNSF, grant 200021_137681. Please contact Dieter Rickenmann (dieter.rickenmann@wsl.ch) if you are interested in the data used in this paper. The manuscript was improved with the feedbacks of the Associate Editor Christophe Ancey, Jonathan B. Laronne and two anonymous reviewers.

References

Almedeij, J. H., and P. Diplas (2003), Bedload transport in gravel-bed streams with unimodal sediment, *J. Hydraul. Eng.*, *129*(11), 896–904, doi:10.1061/(ASCE) 0733-9429(2003)129:11(896).

Ancey, C., F. Bigillon, P. Frey, and R. Ducret (2003), Rolling motion of a bead in a rapid water stream, *Phys. Rev. E*, *67*(1), 011303, doi: 10.1103/PhysRevE.67.011303.

Ancey, C., P. Bohorquez, and E. Bardou (2014), Sediment transport in mountain rivers, *ERCOFTAC Bull.*, *100*, 37–52.

Ancey, C., P. Bohorquez, and J. Heyman (2015), Stochastic interpretation of the advection-diffusion equation and its relevance to bed load transport, *J. Geophys. Res. Earth Surf.*, *120*, 2529–2551, doi:10.1002/2014JF003421.

Barrière, J., A. Krein, A. Oth, and R. Schenkluhn (2015), An advanced signal processing technique for deriving grain size information of bed-load transport from impact plate vibration measurements, *Earth Surf. Process. Landforms*, *40*, 913–924, doi:10.1002/esp.3693.

Barry, J. J., J. M. Buffington, and J. G. King (2004), A general power equation for predicting bed load transport rates in gravel bed rivers, *Water Resour. Res.*, *40*, W10401, doi:10.1029/2004WR003190.

Belleudy, P., A. Valette, and B. Graff (2010), Passive hydrophone monitoring of bedload in river beds: First trials of signal spectral analyses, *Sci. Invest. Rep. 5091*, pp. 67–84. [Available at: http://pubs.usgs.gov/sir/2010/5091/.]

Beylich, A. A., and K. Laute (2014), Combining impact sensor field and laboratory flume measurements with other techniques for studying fluvial bedload transport in steep mountain streams, *Geomorphology*, *218*, 72–87, doi:10.1016/j.geomorph.2013.09.004.

Bogen, J., and K. Møen (2003), Bed load measurements with a new passive acoustic sensor, in *Erosion and Sediment Transport Measurement in Rivers: Trends and Explanation (Proceedings of the Oslo Workshop, June 2002)*, IAHS Publ., vol. 283, edited by J. Bogen, T. Fergus, and D. E. Walling, pp. 181–182, IAHS.

Bunte, K., K. W. Swingle, and S. R. Abt (2007), Guidelines for using bedload traps in coarse-bedded mountain streams: Construction, installation, operation, and sample processing, *Tech. Rep. RMRS-GTR-191*, Dep. of Agric., For. Serv., Rocky Mt. Res. Stn., Fort Collins, Colo.

Burtin, A., L. Bollinger, J. Vergne, R. Cattin, and J. L. Nábělek (2008), Spectral analysis of seismic noise induced by rivers: A new tool to monitor spatiotemporal changes in stream hydrodynamics, *J. Geophys. Res.*, *113*, B05301, doi:10.1029/2007JB005034.

Burtin, A., R. Cattin, L. Bollinger, J. Bollinger, J. Vergne, P. Steer, A. Robert, N. Findling, and C. Tiberi (2011), Towards the hydrologic and bed load monitoring from high-frequency seismic noise in a braided river: The "torrent de St Pierre", French Alps, *J. Hydrol.*, *408*, 43–53, doi:10.1016/j.jhydrol.2011.07.014.

Chatanantavet, P., K. X. Whipple, M. A. Adams, and M. P. Lamb (2013), Experimental study on coarse grain saltation dynamics in bedrock channels, *J. Geophys. Res. Earth Surf.*, *118*, 1161–1176, doi:10.1002/jgrf.20053.

Comiti, F., and L. Mao (2012), Recent advances on the dynamics of steep channels, in *Gravel Bed Rivers 7: Processes, Tools, Environments*, edited by M. Church, P. Biron, and A. Roy, pp. 353–377, Wiley-Blackwell, Chichester.

Dell 'Agnese, A., L. Mao, and F. Comiti (2014), Calibration of an acoustic pipe sensor through bedload traps in a glacierized basin, *Catena*, *121*, 222–231, doi:10.1016/j.catena.2014.05.021.

Downing, J. (2010), Acoustic gravel-momentum sensor, *USGS Sci. Invest. Rep. 5091*, pp. 143–158. [Available at: http://pubs.usgs.gov/sir/2010/5091/.]

Einstein, H. A. (1937), Bedload transport as a probability problem, in *Sedimentation*, edited by H. W. Shen, pp. 1–105, Colo. State Univ., Fort Colins.

Emmett, W. W. (1980), *A Field Calibration of the Sediment-Trapping Characteristics of the Helley-Smith Bedload Sampler*, 44 pp., U.S. Geol. Surv. Prof. Pap. 1139, Wash.

Esbensen, K. H., P. K. Ade, J. F. Zuta, J. Bogen, and K. Møen (2007), Acoustic chemometrics of complex natural systems: Flume test rig feasibility studies for monitoring river bed-load sediment transportation processes, *J. Chemomet.*, *21*(10–11), 459–473, doi:10.1002/cem.1076.

Etter, M. (1996), Zur Erfassung des Geschiebetransportes mit Hydrophonen ('Recording bedload transport with hydrophones'), PhD thesis, Univ. of Berne, Berne, Switzerland, Swiss Federal Research Institute WSL, Birmensdorf, Switzerland.

Geay, T. (2013), Mesure acoustique passive du transport par charriage dans les rivières ('Passive acoustic measurement of bedload transport'), PhD thesis, Univ. Joseph Fourrier de Grenoble, Grenoble, France.

Gimbert, F., V. C. Tsai, M. P. Lamb, F. Gimbert, V. C. Tsai, and M. P. Lamb (2014), A physical model for seismic noise generation by turbulent flow in rivers, *J. Geophys. Res. Earth Surf.*, *119*, 2209–2238, doi:10.1002/2014JF003201.

Gomez, B., R. L. Naff, and D. W. Hubbell (1989), Temporal variations in bedload transport rates associated with the migration of bedforms, *Earth Surf. Process. Landforms*, *14*, 135–156.

Gray, J. R., J. B. Laronne, and J. D. G. Marr (2010), Bedload-surrogate monitoring technologies, *Tech. Rep.*, U.S. Geol. Surv. 2010–5091. [Available at; http://pubs.usgs.gov/sir/2010/5091/.]

Hayward, J. (1980), Hydrology and stream sediments in a mountain catchment, PhD thesis, Special Publ. 17, Tussock Grass-lands and Mt. Lands Inst., Lincoln College, Canterbury, New Zealand.

Helley, E. J., and W. Smith (1971), Development and calibration of a pressure-difference bedload sampler, *U.S. Geol. Surv. Open File Rep. 73-108*, U.S. Geol. Surv., Water Resour. Div., Menlo Park, Calif.

Hilldale, R. C., W. O. Carpenter, B. Goodwiller, J. P. Chambers, T. J. Randle, D. Wre, and M. Asce (2014), Installation of impact plates to continuously measure bed load: Elwha River, Washington, USA, *J. Hydraul. Eng.*, *141*(3), doi:10.1061/(ASCE)HY.1943-7900. [Available at: http://ascelibrary.org/doi/abs/10.1061/(ASCE)HY.1943-7900.0000975.]

Julien, P. Y., and B. Bounvilay (2013), Velocity of rolling bed load particles, *J. Hydraul. Eng.*, *139*, 177–186, doi:10.1061/(ASCE)HY.1943-7900.0000657.

Krein, A., H. Klinck, M. Eiden, W. Symader, R. Bierl, L. Hoffmann, and L. Pfister (2008), Investigating the transport dynamics and the properties of bedload material with a hydro-acoustic measuring system, *Earth Surf. Process. Landforms*, *33*, 152–163, doi:10.1002/esp.1576.

Lajeunesse, E., L. Malverti, and F. Charru (2010), Bed load transport in turbulent flow at the grain scale: Experiments and modeling, *J. Geophys. Res.*, *115*, F04001, doi:10.1029/2009JF001628.

Lenzi, M. A., L. Mao, G. Asti, F. Comiti, and G. R. Scussel (2004), Impact of sediment supply on bed load transport in a high-altitude alpine torrent, in *Int. Symposion Interpraevent*, pp. Bd, 1, III/171–182, Interpraevent Tagungspublikation, Riva, Trient.

Mao, L., R. Carrillo, C. Escauriaza, and A. Iroume (2016), Flume and field-based calibration of surrogate sensors for monitoring bedload transport, *Geomorphology*, *253*, 10–21, doi:10.1016/j.geomorph.2015.10.002.

Mizuyama, T., et al. (2010a), Calibration of a passive acoustic bedload monitoring system in Japanese mountain rivers, in *Bedload-Surrogate Monitoring Technologies, U.S. Geol. Surv. Sci. Invest. Rep. 2010-5091*, edited by J. R. Gray, J. B. Laronne, and J. D. Marr, 2010 ed., pp. 296–318, U.S. Geol. Surv., Reston, Va.

Mizuyama, T., A. Oda, J. B. Laronne, M. Nonaka, and M. Matsuoka (2010b), Laboratory tests of a japanese pipe geophone for continuous acoustic monitoring of coarse bedload, in *Bedload-Surrogate Monitoring Technologies*, *U.S. Geol. Surv. Sci. Invest. Rep. 2010-5091*, edited by J. R. Gray, J. B. Laronne, and J. D. Marr, 2010 ed., pp. 319–335, U.S. Geol. Surv., Reston, Va.

Monsalve, A., D. Yager, J. M. Turowski, and D. Rickenmann (2016), A probabilistic formulation of bed load transport to include spatial variability of flow and surface grain size distributions, *Water Resour. Res.*, *52*, 3579–3598, doi:10.1002/2015WR017694.

Nitsche, M., D. Rickenmann, J. M. Turowski, A. Badoux, and J. W. Kirchner (2011), Evaluation of bedload transport predictions using flow resistance equations to account for macro-roughness in steep mountain streams, *Water Resour. Res.*, *47*, W08513, doi:10.1029/2011WR010645.

Nitsche, M., D. Rickenmann, J. M. Turowski, A. Badoux, and J. W. Kirchner (2012), Macroroughness and variations in reach-averaged flow resistance in steep mountain streams, *Water Resources Research*, *48*, W12518, doi:10.1029/2012WR012091.

Rickenmann, D. (2001), Comparison of bed load transport in torrent and gravel bed streams, *Water Resour. Res.*, *37*(12), 3295–3305, doi:10.1029/2001WR000319.

Rickenmann, D., and B. Fritschi (2010), Bedload transport measurements using piezoelectric impact sensors and geophones, in *Bedload-Surrogate Monitoring Technologies*, *U.S. Geol. Surv. Sci. Invest. Rep. 2010-5091*, edited by J. R. Gray, J. B. Laronne, and J. D. Marr, 2010 ed., pp. 407–423, U.S. Geol. Surv., Reston, Va.

Rickenmann, D., J. M. Turowski, B. Fritschi, A. Klaiber, and A. Ludwig (2012), Bedload transport measurements at the Erlenbach stream with geophones and automated basket samplers, *Earth Surf. Process. Landforms*, *37*, 1000–1011, doi:10.1002/esp.3225.

Rickenmann, D., et al. (2014), Bedload transport measurements with impact plate geophones: Comparison of sensor calibration in different gravel-bed streams, *Earth Surf. Process. Landforms*, *39*, 928–942, doi:10.1002/esp.3499.

Schneider, J. M., J. M. Turowski, D. Rickenmann, R. Hegglin, S. Arrigo, L. Mao, and J. W. Kirchner (2014), Scaling relationships between bed load volumes, transport distances, and stream power in steep mountain channels, *J. Geophys. Res. Earth Surf.*, *119*, 553–549, doi: 10.1002/2013JF002874.

Schneider, J. M., D. Rickenmann, J. M. Turowski, K. Bunte, and J. W. Kirchner (2015), Applicability of bed load transport models for mixed-size sediments in steep streams considering macro-roughness, *Water Resour. Res.*, *51*, 5260–5283, doi:10.1002/2014WR016417.

Thorne, P. D. (1985), The measurement of acoustic noise generated by moving artificial sediments, *J. Acoust. Soc. Am.*, *78*(3), 1013–1023.

Thorne, P. D. (1986), Laboratory and marine measurements on the acoustic detection of sediment transport, *J. Acoust. Soc. Am.*, *80*(3), 899–910.

Travaglini, E., E. Bardou, A. Christophe, and P. Bohorquez (2014), Analysis of sediment transport from recorded signals of sediments in a gravel-bed river: Role of sediment availability, *Eng. Geol. Soc. Territ.*, *3*, 477–481, doi:10.1007/978-3-319-09054-2.

Tsakiris, A. G., A. N. Papanicolaou, and T. Lauth (2014), Signature of bedload particle transport mode in the acoustic signal of a geophone, *J. of Hydraul. Res.*, *52*, 185–204, doi:10.1080/00221686.2013.876454.

Turowski, J. M., and D. Rickenmann (2009), Tools and cover effects in bedload transport observations in the Pitzbach, Austria, *Earth Surf. Process. Landforms*, *34*, 26–37, doi:10.1002/esp.1686.

Turowski, J. M., A. Badoux, and D. Rickenmann (2011), Start and end of bedload transport in gravel-bed streams, *Geophys. Res. Lett.*, *38*, L04401, doi:10.1029/2010GL046558.

Turowski, J. M., M. Böckli, D. Rickenmann, and A. Beer (2013), Field measurements of the energy delivered to the channel bed by moving bed load and links to bedrock erosion, *J. Geophys. Res. Earth Surf.*, *118*, 2438–2450, doi:10.1002/2013JF002765.

Turowski, J. M., C. R. Wyss, and A. R. Beer (2015), Grain size effects on energy delivery to the stream bed and links to bedrock erosion, *Geophys. Res. Lett.*, *42*, 1775–1780, doi:10.1002/2015GL063159.

Wyss, C. R., D. Rickenmann, B. Fritschi, J. M. Turowski, V. Weitbrecht, and R. M. Boes (2014), Bedload grain size estimation from the indirect monitoring of bedload transport with Swiss plate geophones at the Erlenbach stream, in *River Flow 2014*, edited by A. Schleiss, et al., pp. 1907–1912, Taylor and Francis, Lausanne, Switzerland.

Wyss, C. R., D. Rickenmann, B. Fritschi, J. M. Turowski, V. Weitbrecht, and R. M. Boes (2016a), Laboratory flume experiments with the Swiss plate geophone bedload monitoring system: 1. Impulse counts and particle size identification, *Water Resour. Res.*, *52*, doi:10.1002/2015WR018555.

Wyss, C. R., D. Rickenmann, B. Fritschi, J. M. Turowski, V. Weitbrecht, and R. M. Boes (2016b), Measuring bedload transport rates by grain-size fraction using the Swiss plate geophone at the Erlenbach, *J. Hydraul. Eng.*, *142*(5), 1–11, doi:10.1061/(ASCE)HY.1943-7900.0001090.